

Ruthenium and Osmium Complexes of Phosphine-Porphyrin Derivatives as Potential Bimetallic Theranostics: Photophysical Studies

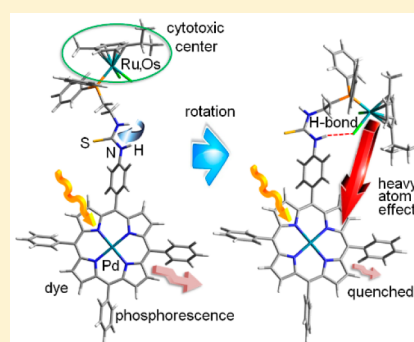
Pierre D. Harvey,^{*,†,‡} Semra Tasan,[‡] Claude P. Gros,^{*,‡} Charles H. Devillers,[‡] Philippe Richard,[‡] Pierre Le Gendre,[‡] and Ewen Bodio^{*,‡}

[†]Département de Chimie, Université de Sherbrooke, Sherbrooke, Québec, Canada J1K 2R1

[‡]ICMUB (UMR CNRS 6302), Université de Bourgogne, 21000 Dijon, France

Supporting Information

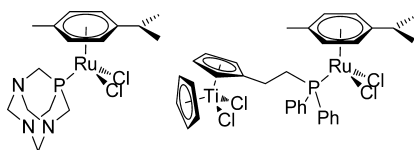
ABSTRACT: A series of (η^6 -*p*-cymene)ruthenium(II)- and osmium(II) complexes of porphyrin-phosphane derivatives have been synthesized as potential bimetallic theranostic candidates. The photophysical and electrochemical properties were investigated, and these species desirably exhibit no or almost no photoinduced intramolecular energy, and electron transfer between the dye and the metallic fragment. These favorable features are mostly associated with the presence of their long chain (i.e., ~ 1 nm) separating the two functional units. Interestingly, a decrease in emission intensity and lifetimes (up to 35-fold) has been observed, which was ascribed to a small heavy atom effect. This effect is possible as a chain folding driven by an intramolecular H-bond (N–H \cdots Cl–M).



INTRODUCTION

The design of trackable therapeutic agents and more generally of theranostics is the subject of intense current interest.¹ Indeed, the combination of an imaging probe with a therapeutic moiety allows for a large scope of applications from the personalized medicine to the understanding of drug mechanisms. Recently, the use of organometallics in theranostic designs, although a relatively newer topic, was reviewed.² One of the popular promising organometallic complexes (and motifs) used in cancer therapy is the now well-known RAPTA-C: [Ru(η^6 -*p*-cymene)Cl₂(pta)] (pta = 1,3,5-triaza-7-phosphatricyclo[3.3.1.1]-decane; Chart 1), along with its

Chart 1. Structures of [Ru(η^6 -*p*-cymene)Cl₂(pta)] (Left) and [(η^5 -Cp)Ti(η^5 -C₅H₄-(CH₂)₄-PPh₂)[Ru(η^6 -*p*-cymene)Cl₂]] (Right)



osmium analogue and their corresponding functionalized derivatives.³ RAPTA-C and its analogues display poor IC50 *in vitro* on cancer cells. However, they have been reported to exhibit very promising antimetastatic properties *in vivo*.^{3c,o} Their mechanism is yet to be clearly established.⁴ Conversely, for the quite strongly bonded phosphine and arene ligands, the chlorido ligands are believed to rapidly interchange with water

molecules. Arene-ruthenium derivatives can react with *N*- and *S*-donors enabling them to bind to both nucleotides and proteins.⁵ Since 2005, more and more studies focus on the processes involving protein targets (e.g., ubiquitin or cathepsin B)⁶ or even small peptides such as glutathione, which is known as a detoxification agent of metal-based drugs contributing to resistance development.⁷ Recently, one of us investigated some bimetallic versions of this ruthenium organometallic synthon along with a titanocene center (Chart 1).^{5b} However, although they are convenient for their marked increased cytotoxic activities, this series suffers, as previous arene-ruthenium derivatives, from the lack of a label to track them *in vitro* and/or *in vivo*.

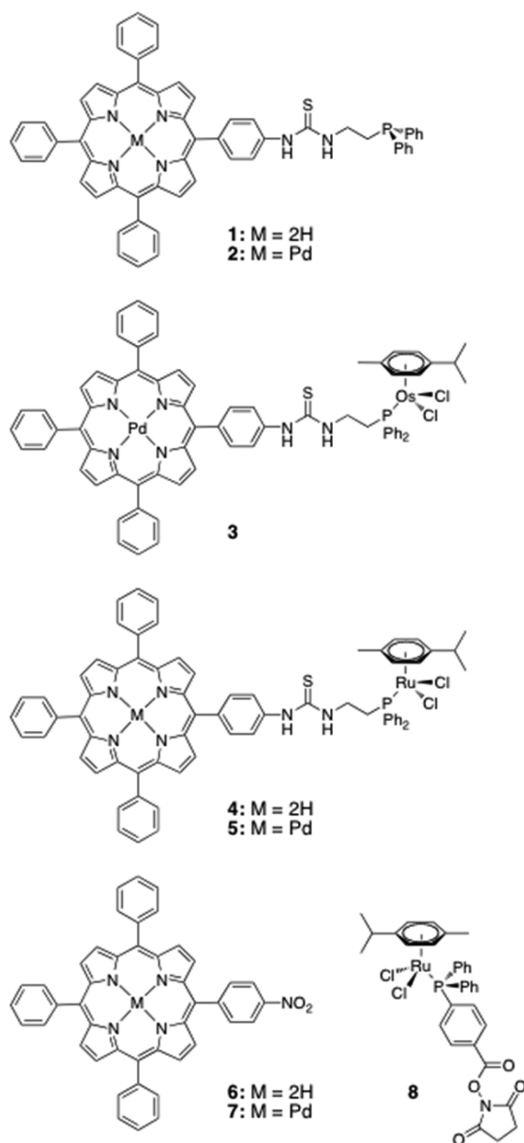
Concurrently, porphyrins and their metallo-derivatives have been the subject of intense research in the field of photodynamic therapy⁸ and optical imaging, making them obvious candidates as theranostic agents.⁹ It is also well-known that the use of a heavy atom such as gold(III) inside the porphyrin rings and derivatives demonstrate a good ability to act as anticancer agents.¹⁰ This also holds true for palladium(II) (here via photocytotoxicity; photodynamic therapy)¹¹ and palladium(III).¹² Based on these previous investigations, it now appears as a normal and convenient extension to design multifunctional theranostic agents, here combining both the imaging and photodynamic properties of porphyrins, specifically palladium(II) porphyrins, and the cancer cytotoxicity of

Received: December 5, 2014

the complexes related to the well-known arene-ruthenium derivatives. This trait would result in the conception of an “optical bi-theranostic” (two modalities for therapy and one for optical imaging). One of the key issues is that although the bricks of construction appear ideal for their own function, intramolecular interactions between the two moieties profoundly altering their activities are always possible and must be addressed prior to design and testing. In the case of fluorescence/phosphorescence imaging and photodynamic therapy, such interactions between the two fragments are primarily due to photoinduced energy, electron, and atom transfers from one unit to the other. It is this preliminary issue we would like to address.

We now report the preparation, the photophysical and electrochemical properties of a series of (η^6 -*p*-cymene)-ruthenium(II) and osmium(II) complexes of porphyrin-phosphane derivatives (employed as dyes) as potential bimetallic theranostics (Chart 2). In order to preclude or significantly reduce intermetallic complex interactions, a long

Chart 2. Structures of the Investigated Bimetallic Compounds 1–5 along with Model Compounds 6–8



spacing chain between the moieties is used. The choice of a thiourea unit within the spacer is justified by the facile synthesis and its high stability *in vivo*. These targets exhibit desirably no or almost no photoinduced intramolecular atom, energy, and electron transfer between the dye and the metallic fragment. This sought behavior is mainly due to the presence of a long chain. However, a quenching (up to 35-fold) can be noted and is due to a small heavy atom effect. This effect is rendered possible because of a chain folding driven by an intramolecular H-bond (N–H...Cl–M).

EXPERIMENTAL SECTION

Chemicals and Reagents. Solvents were dried and distilled under argon before use. All the analysis were performed at the *Plateforme d'Analyses Chimiques et de Synthèse Moléculaire de l'Université de Bourgogne*. Synthesis of compound 1, 2, 6–8 was done as previously reported (see Supporting Information (SI) for details).¹³

[η^6 -*p*-Cymene](palladium(II) 5-(4-(N-(2-(diphenylphosphino)ethyl)thiocarbamido)-aminophenyl)-10,15,20-triphenylporphyrin)-OsCl₂] (3). The reaction was carried out under an argon atmosphere. Porphyrin phosphine derivative 2 (99 mg, 0.10 mmol, 1.0 equiv) and [OsCl₂(η^6 -*p*-cymene)]₂ (39 mg, 0.05 mmol, 0.5 equiv) were dissolved in dichloromethane (3 mL). The resulting mixture was stirred for 3 h at room temperature. The completion of the reaction was monitored by ³¹P NMR (202.5 MHz, 300 K). The solvent was removed under reduced pressure. The osmium complex 3 was isolated as a bright red powder (136 mg, 98%). UV–vis (THF): λ_{max} (nm) (ϵ , 10³ M⁻¹ cm⁻¹) 416 (249), 524 (26), 554 (3). IR: $\bar{\nu}$ (cm⁻¹) 297 ($\nu_{\text{Os-Cl}}$), 795 ($\nu_{\text{C=S}}$), 1352 ($\nu_{\text{C-N}}$), 1508 ($\nu_{\text{N-C-N}}$), 3049 ($\nu_{\text{N-H}}$). ¹H NMR (500.13 MHz, DMSO-*d*₆): δ (ppm) 0.79 (d, 6H, ³J = 6.9 Hz, CH(CH₃)₂), 1.89 (s, 3H, CH₃), 2.17 (hept, 1H, ³J = 6.9 Hz, CH(CH₃)₂), 3.02 (m, 2H, NH–CH₂), 3.44 (m, 2H, CH₂–PPh₂), 5.44 (d, 2H, ³J = 5.9 Hz, *p*-cymene-Os), 5.56 (d, 2H, ³J = 5.9 Hz, *p*-cymene-Os), 7.46–7.58 (m, 6H, *o*- and *p*-PPh₂), 7.63–7.89 (m, 16H, *m*-PPh₂ + NH + C₆H₄NH + H_{Ar}), 8.05 (d, 2H, ³J = 8.4 Hz, C₆H₄NH), 8.14–8.17 (m, 7H, NH + H_{Ar}), 8.77–8.87 (m, 8H, H β). ¹³C{¹H} NMR (125.8 MHz, CDCl₃): δ (ppm) 180.1, 141.0, 140.9, 140.8, 140.6, 136.0, 134.1, 133.7, 133.1, 132.0, 131.5, 131.3, 131.0, 130.4, 130.4, 130.3, 128.8, 128.4, 128.1, 128.0, 127.0, 121.8, 127.7, 121.6, 120.9, 97.3, 86.5, 81.5, 78.1, 54.9, 29.2, 21.3, 16.8, 16.3. ³¹P{¹H} NMR (202.5 MHz, DMSO-*d*₆): δ (ppm) – 21.1. HR-MS (MALDI-TOF): *m/z* calcd for C₆₉H₅₇Cl₂N₆OsPPdS – HCl – Cl⁺: 1329.2677 [M – HCl – Cl]⁺. Found: 1329.2627. HR-MS (ESI): *m/z* calcd for C₆₉H₅₇Cl₂N₆OsPPdS – HCl – Cl⁺: 1329.26768 [M – HCl – Cl]⁺. Found: 1329.26037.

[5-(4-(N-(2-(Diphenylphosphino)ethyl)thiocarbamido)-aminophenyl)-10,15,20-triphenylporphyrin]-RuCl₂] (4). The reaction was carried out inside a glovebox. Porphyrin phosphine derivative 1 (90 mg, 0.10 mmol, 1.0 equiv) and [RuCl₂(η^6 -*p*-cymene)]₂ (31 mg, 0.05 mmol, 0.5 equiv) were dissolved in dichloromethane (5 mL). The resulting mixture was stirred for 16 h at room temperature. The completion of the reaction was monitored by ³¹P NMR (202.5 MHz, 300 K). The solvent was removed under reduced pressure. The ruthenium complex 4 was isolated as a bright purple powder (121 mg > 99%). UV–vis (THF): λ_{max} (nm) (ϵ , 10³ M⁻¹ cm⁻¹) 418 (318), 515 (19), 550 (10), 592 (6), 649 (4). IR: $\bar{\nu}$ (cm⁻¹) 289 ($\nu_{\text{Ru-Cl}}$), 798 ($\nu_{\text{C=S}}$), 1349 ($\nu_{\text{C-N}}$), 1537 ($\nu_{\text{N-C-N}}$), 3310 ($\nu_{\text{N-H}}$). ¹H NMR (300.13 MHz, DMSO-*d*₆): δ (ppm) – 2.88 (br s, 2H, NH_{Porph}), 0.76 (d, 6H, ³J = 6.9 Hz, CH(CH₃)₂), 1.79 (s, 3H, CH₃), 2.26–2.37 (m, 1H, CH(CH₃)₂), 2.87–3.04 (m, 2H, NH–CH₂), 3.33–3.55 (m, 2H, CH₂–PPh₂), 5.26 (d, 2H, ³J = 6.2 Hz, *p*-cymene-Ru), 5.44 (d, 2H, ³J = 6.2 Hz, *p*-cymene-Ru), 7.52–8.07 (m, 23H, PPh₂ + 2NH + C₆H₄ + H_{Ar}), 8.09–8.24 (m, 8H, C₆H₄NH + H_{Ar}), 8.81–8.92 (m, 8H, H β). ¹³C{¹H} NMR (75.5 MHz, DMSO-*d*₆): δ (ppm) 141.2, 134.9, 134.5, 134.2, 133.2, 132.0, 131.4, 131.2, 130.8, 130.4, 128.7, 128.5, 128.1, 126.9, 126.0, 123.7, 121.0, 120.0, 89.6, 86.0, 85.3, 54.9, 21.0, 17.0, 16.7. ³¹P{¹H} NMR (121.5 MHz, DMSO-*d*₆): δ (ppm) 19.9 ppm. HR-MS (MALDI-TOF): *m/z* calcd for C₆₉H₅₉Cl₂N₆PRuS – HCl – Cl⁺: 1135.3237 [M – HCl – Cl]⁺. Found: 1135.3237. HR-MS (ESI): *m/z*

calcd for $C_{69}H_{59}Cl_2N_6PRuS - HCl - Cl^{+}$: 1135.3237 [M - HCl - Cl] $^{+}$. Found: 1135.3255.

[(*η*⁶-*p*-Cymene)(palladium(II) 5-(4-(*N*-(2-(diphenylphosphino)ethyl)thiocarbamido)amino phenyl)-10,15,20-triphenylporphyrin)-RuCl₂] (5). The reaction was carried out under an argon atmosphere. Porphyrin phosphine derivative 2 (97 mg, 0.10 mmol, 1.0 equiv) and [RuCl₂(*η*⁶-*p*-cymene)]₂ (30 mg, 0.05 mmol, 0.5 equiv) were dissolved in distilled dichloromethane (3.5 mL). The resulting mixture was stirred for 3 h at room temperature. The completion of the reaction was monitored by ³¹P NMR (202.5 MHz, 300 K). The solvent was removed under reduced pressure. The ruthenium complex 5 was isolated as a bright red powder (125 mg, 99%). UV-vis (THF): λ_{max} (nm) (ε, 10³ M⁻¹ cm⁻¹) 416 (249), 523 (26), 554 (3). IR: ν̄ (cm⁻¹) 293 (ν_{Ru-Cl}), 796 (ν_{C=S}), 1352 (ν_{C-N}), 1508 (ν_{N-C-N}), 3049 (ν_{N-H}). ¹H NMR (500.13 MHz, DMSO-*d*₆): δ (ppm) 0.74 (d, 6H, ³J = 6.9 Hz, CH(CH₃)₂), 1.77 (s, 3H, CH₃), 2.31 (hept, 1H, ³J = 6.9 Hz, CH(CH₃)₂), 2.90 (m, 2H, NH-CH₂), 3.40 (m, 2H, CH₂-Ph), 5.22 (d, 2H, ³J = 6.2 Hz, *p*-cymene-Ru), 5.40 (d, 2H, ³J = 6.2 Hz, *p*-cymene-Ru), 7.51–7.59 (m, 6H, *o*- and *p*-PPh₂), 7.64–7.93 (m, 16H, *m*-PPh₂ + NH + C₆H₄NH + H_{Ar}), 8.04 (d, 2H, ³J = 8.4 Hz, C₆H₄NH), 8.10–8.17 (m, 7H, NH + H_{Ar}), 8.77–8.87 (m, 8H, H_β). ¹³C{¹H} NMR (125.8 MHz, DMSO-*d*₆): δ (ppm) 180.0, 140.9, 140.8, 140.7, 140.6, 139.0, 136.0, 134.1, 133.7, 133.1, 132.5, 132.2, 131.4, 131.3, 131.1, 131.0, 130.4, 130.3, 128.8, 128.5, 128.1, 128.0, 127.0, 121.8, 121.6, 121.5, 121.0, 106.3, 93.9, 89.8, 86.3, 85.5, 54.8, 29.4, 21.4, 20.9, 16.9. ³¹P{¹H} NMR (202.5 MHz, DMSO-*d*₆): δ (ppm) 19.9. HR-MS (MALDI-TOF): *m/z* calcd for C₆₉H₅₇Cl₂N₆PPdRuS - 2Cl $^{+}$: 1240.2136 [M - 2Cl] $^{+}$. Found: 1240.2148. HR-MS (ESI): *m/z* calcd for C₆₉H₅₇Cl₂N₆PPdRuS - HCl - Cl $^{+}$: 1239.21284 [M - HCl - Cl] $^{+}$. Found: 1239.21031.

Instrumentation. ¹H (300.13, 500.13, or 600.13 MHz), ¹³C (75.5, 125.8, or 150.9 MHz), ³¹P (121.5, 202.5, or 242.9 MHz) NMR spectra were recorded on a Bruker 300 Bruker Avance III, a Bruker 500 Avance III, or on a Bruker 600 Avance II spectrometer. Chemical shifts are quoted in parts per million (δ) relative to TMS (¹H and ¹³C), using the residual protonated solvent (¹H) or the deuterated solvent (¹³C) as an internal standard. Alternatively, 85% H₃PO₄ (³¹P) was used as external standard. Coupling constants are reported in Hertz and represent proton–proton coupling. Mass spectra were obtained by MALDI-TOF with a Bruker DALTONICS Ultraflex II spectrometer. High-resolution mass measurements were carried out using a Bruker DALTONICS Ultraflex II spectrometer (HR-MS MALDI-TOF) or Bruker microTOF-Q ESI-MS and LTQ Orbitrap XL (Thermo) mass spectrometers and low-resolution mass measurements were carried out using an amazon SL (Bruker) mass spectrometer. Far infrared spectra were recorded with IR FT Bruker Vertex 70v spectrophotometer. Absorption spectra were recorded on a VARIAN CARY 50 spectrometer.

Absorption, Emission, and Excitation Spectra. All samples were prepared in 2-methyl-tetrahydrofuran, 2MeTHF, which was distilled over CaH₂ under nitrogen. The absorption spectra were recorded at 298 and 77 K using a Varian Cary 300 spectrophotometer and a HP-8453 diode array spectrophotometer, respectively, at the *Université de Sherbrooke*, or on a JASCO V630 Bio spectrometer at the *Université de Bourgogne* at 298 K. Molar absorptivity determination was verified by linear least-squares fit of values obtained from at least three independent solutions at varying concentrations with absorbance ranging from 0.01 to 2.6. Steady-state emission and excitation spectra were recorded at 298 and 77 K in a 1.0 cm capped quartz cell and a 5.0 mm (i.d.) NMR tube inserted into quartz EPR Dewar filled with liquid N₂, respectively. Emission spectra were obtained by exciting at the lowest energy absorption maxima using a Horiba Jobin Yvon Fluorolog spectrofluorometer equipped with double monochromators.

Fluorescence Quantum Yield and Lifetimes. The measurements of the emission quantum yields were performed in 2-MeTHF at 298 K. Three different measurements (i.e., different solutions) were prepared for each photophysical datum (quantum yields and lifetimes). For measurements at 298 K, samples were prepared under inert atmosphere (in a glovebox, P_{O₂} < 10 ppm). The sample and the standard concentrations were adjusted to obtain an absorbance of 0.05

or less. This absorbance was adjusted to be the same as much as possible for the standard and the sample for a measurement. Each absorbance value was measured five times for better accuracy in the measurements of the quantum yields. The equation $\Phi_s = \Phi_r(F_r/F_s)(I_r/I_s)(n_s/n_r)^2$ was used to calculate the relative quantum yield of each of the sample, where Φ is the absolute quantum yield of the reference, n is the refractive index of the solvent, F is the absorbance ($F = 1 - 10^{-A}$, where A is the absorbance) at the excitation wavelength, and I is the integrated area under the corrected emission curve. The subscripts s and r refer to the sample and reference, respectively. A solution of *meso*-tetraphenylporphyrin (H₂TPP) in 2-MeTHF ($\Phi_F = 0.11$)¹⁴ was used as the external reference. The emission lifetimes in the 1 to 10 ns range were measured on a TimeMaster model TM-3/2003 apparatus from PTI. The source was a nitrogen laser with high-resolution dye laser (fwhm ~ 1400 ps), and the excited lifetimes were obtained from deconvolution or distribution lifetimes analysis.

Calculations. Density functional theory (DFT) calculations were performed with Gaussian 09¹⁵ at the *Université de Sherbrooke* with the Mammouth supercomputer supported by *Le Réseau Québécois De Calculs Hautes Performances*. The DFT geometry optimizations¹⁶ were carried out using the B3LYP method. A 6-31g* basis set was used for C, H, N, P, and Cl atoms.¹⁷ VDZ (valence double ζ) with SBKJC effective core potentials were used for all Pd and Ru atoms.¹⁷ A THF solvent field was applied to all calculations. A frequency calculation was performed on the optimized geometries in order to verify the nature of the stationary point. The frequency calculations showed no imaginary frequencies indicating that the stationary points found are true minima.

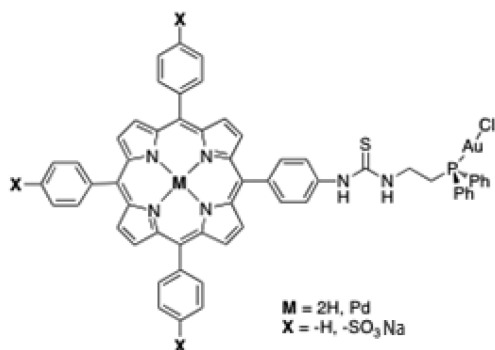
X-ray Analysis. Intensity data for compound 8 were collected on a Nonius Kappa APEX II at 115 K. Using Olex2,¹⁸ the structure was solved with the ShelXS¹⁹ structure solution program using Direct Methods and refined with the XL¹⁹ refinement package using Least Squares minimization. All non-hydrogen atoms were refined with anisotropic thermal parameters. Hydrogen atoms were included in their calculated positions and refined with a riding model. Crystallographic data are reported in the SI (Table S26).

Electrochemistry. Tetra-*n*-butylammoniumhexafluorophosphate (TBAPF₆) was synthesized by mixing stoichiometric amounts of tetra-*n*-butylammonium hydroxide (Alfa-Aesar, 40% w/w aq soln) and hexafluorophosphate acid (Alfa-Aesar, ca. 60% w/w aq soln). After filtration, the salt was recrystallized three times in ethanol and dried at 80 °C during at least 2 days. All electrochemical manipulations were performed using Schlenk techniques in an atmosphere of dry oxygen-free argon at room temperature ($T = 20 \pm 3$ °C). The supporting electrolyte was degassed under vacuum before use and then dissolved to a concentration of 0.1 mol/L. Voltammetric analyses were carried out in a standard three electrode cell, with an Autolab PGSTAT 302 N potentiostat, connected to an interfaced computer that employed Electrochemistry Nova software. The reference electrode was a saturated calomel electrode (SCE) separated from the analyzed solution by a sintered glass disk filled with the background solution. The auxiliary electrode was a platinum wire separated from the analyzed solution by a sintered glass disk filled with the background solution. For all voltammetric measurements, the working electrode was a platinum disk electrode (Ø = 2 mm). In these conditions, when operating in CH₂Cl₂ (0.1 M TBAPF₆), the formal potential for the Fc⁺/Fc couple was found to be +0.44 V vs SCE.

RESULTS AND DISCUSSION

We previously described the synthesis of new porphyrinophosphine-gold derivatives (Chart 3). Some of these compounds then reported as potential theranostics gave interesting results both in term of photophysical properties (*in vitro* imaging experiments were easily performed) and cytotoxic activity.^{13a} This series is now expanded by synthesizing the corresponding arene-ruthenium and arene-osmium derivatives (Chart 2). First, the porphyrin-phosphine ligands 1 and 2 (Scheme 1) were prepared. In order to preclude or significantly reduce

Chart 3. Structures of the Gold Complexes



intermetallic complex interactions, a long spacing chain between the moieties is employed.

These ligands were efficiently synthesized in only four steps involving: (i) mononitration of the tetraphenylporphyrin (TPP), (ii) reduction of the nitro group by mercaptoethanol, (iii) reaction with thiophosgene to obtain the corresponding isothiocyanate compounds, and finally, (iv) coupling with 2-aminoethyldiphenylphosphine. For the Pd-metalated porphyrin-phosphine, an additional complexation step was used between the nitration and the reduction ones. The ruthenium and osmium derivatives were easily obtained by reacting the corresponding phosphine derivatives using 0.5 equiv of dichlorido(*p*-cymene)metal dimer in dichloromethane for 3.5 h at room temperature. The three complexes were obtained quantitatively by simple evaporation of the solvent under reduced pressure. The metalation reaction was monitored by UV-vis spectroscopy and ^{31}P NMR spectrometry, and these complexes were fully characterized by 1H and ^{13}C NMR, IR, and HRMS mass spectrometry. The molecular ions of the free base porphyrins **1** and **4** and metal complexes **2**, **3**, **5** were observed as the most intense peak in the mass spectra for all cases. The data agree well with the expected molecular formula. For example, the HR-MS MALDI-TOF mass spectrum of **5** exhibits the parent-ion peak at $m/z = 1240.2148$ (calcd for $C_{69}H_{57}N_6PPdRuS$, $[M - 2Cl]^+ m/z 1240.2136$) (SI).

Notably, the chlorido ligands turned out to be exchangeable in solution. Interestingly, this phenomenon was clearly

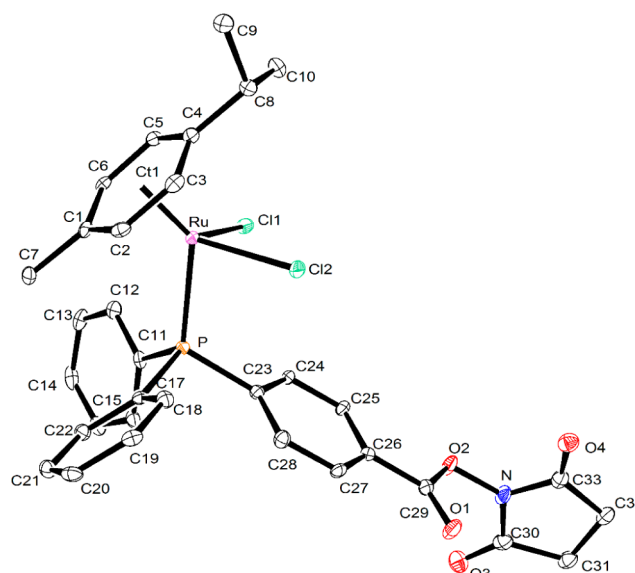
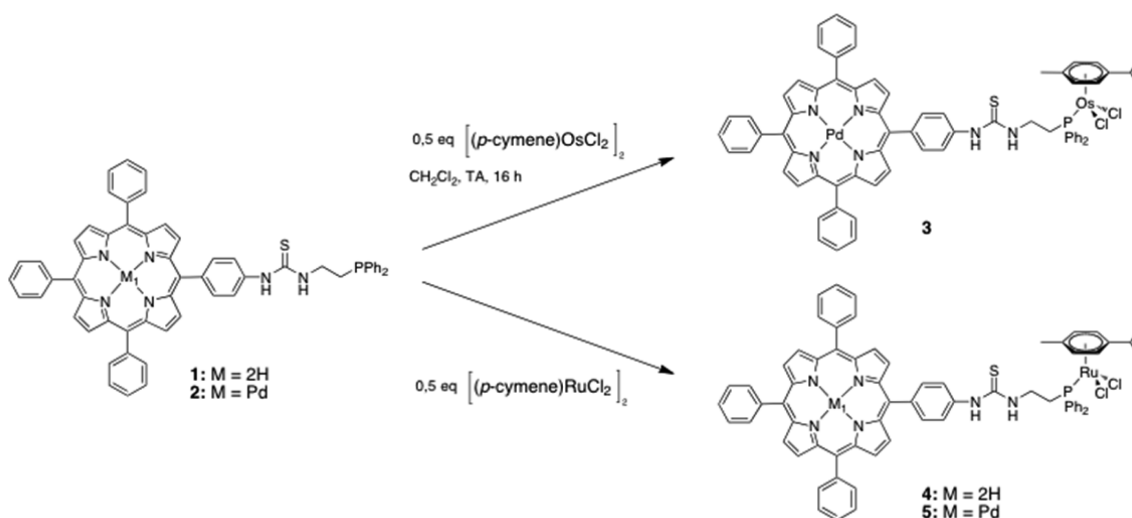


Figure 1. ORTEP view of complex **8**. Selected bonds (Å) and angles (deg): Ru–Ct1 1.702(7), Ru–Cl1 2.4139(16), Ru–Cl2 2.427(2), Ru–P 2.3621(17), Ct1–Ru–Cl1 125.66(25), Ct1–Ru–Cl2 124.89(24), Ct1–Ru–P 131.94(22), Cl1–Ru–Cl2 88.71(7), Cl1–Ru–P 86.08(6), Cl2–Ru–P 85.60(7).

evidenced when DMSO- d_6 was used as the solvent for the 1H NMR spectra. Indeed, a mono-DMSO adduct was observed in the spectra. This exchange was studied for the Ru(II)-complexes by variable temperature NMR experiment (see SI for details). Indeed, all complexes were found in their mono-DMSO adduct form at ~ 90 °C. The lability of the chlorido ligands is well-known in the literature, and some researchers have reported that this exchange could also occur with water molecules. In anticancer studies, the corresponding aqua complex has been hypothesized as being the active form of the complex. Nevertheless, the kinetics of this exchange is very dependent on the complex. In this work, this exchange is very slow at room temperature. For instance, 40 days were needed for the completion of the monosubstitution with DMSO. Moreover, we previously investigated the stability of the model compound **8** in a mixture containing cell culture medium at 37

Scheme 1. Synthesis of 3–5



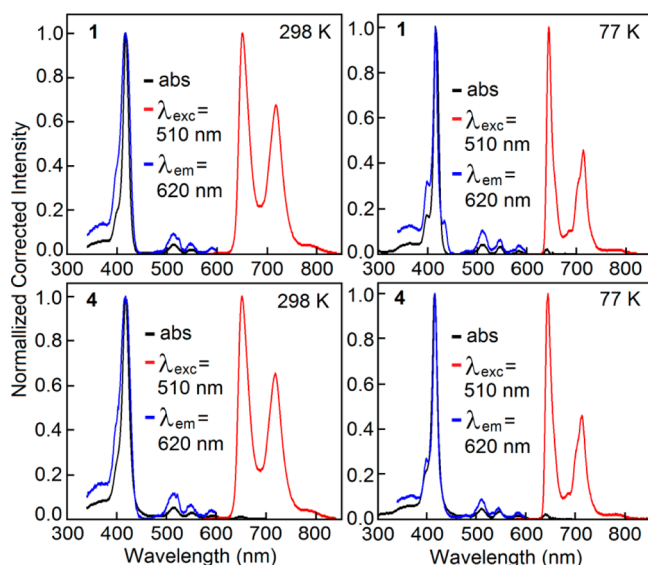


Figure 2. Absorption (black), emission (red), and excitation (blue) spectra of **1** and **4** in 2-MeTHF at 298 and 77 K. The instrumental limit of the excitation spectra is 600 nm.

°C, and no change was observed up to 10 days.^{13b} Noteworthy, a UV–visible study combined with mass spectrometry of **3** and **5** dissolved in a DMSO/water mixture (1/99 v/v) for 3 days at 37 °C was performed, and no degradation of the complexes was observed (see SI for details).

Crystallography. Compound **8** was synthesized as a model for the ruthenium(II) moiety for further investigation in photophysics and electrochemistry. We previously described the synthesis of this complex,^{13b} but its X-ray structure was never reported. A suitable monocrystal for X-ray diffraction was obtained by slow diffusion of pentane in a solution of **8** in dichloromethane. This structure clearly confirmed the identification of the complex and highlights the characteristic “piano stool” conformation of arene–ruthenium complexes (Figure 1).

Spectroscopic and Photophysical Studies. The absorption spectra of the free base-containing porphyrins, [Fb], **1** and **4** in 2-MeTHF exhibit the expected intense Soret band ($S_0 \rightarrow S_2$) at ~ 418 nm and the Q-bands ($S_0 \rightarrow S_1$) at ~ 515 , 550, 592, and 648 nm at 298 K (Figure 2; Table 1).²⁰ For the palladium(II) porphyrin-containing ligand and complexes, [Pdporph], **2**, **3**, and **5**, the Soret and Q-bands are noted as anticipated at ~ 416 nm and ~ 523 and 554 nm, respectively, (298 K; Figure 3; Table 1). The excitation spectra superpose well the absorption, meaning that the emission arises from the dye and not an impurity.

All four dyes are luminescent. The [Fb], **1**, and **4** species exhibit the typical signature generally observed for a

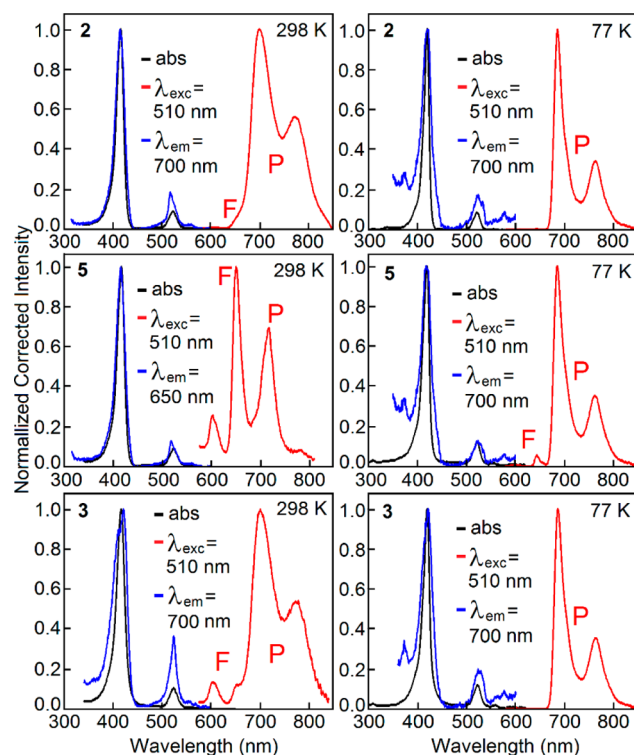


Figure 3. Absorption (black), emission (red), and excitation (blue) spectra of **2**, **3**, and **5** in 2-MeTHF at 298 and 77 K (F = fluorescence; P = phosphorescence). The excitation spectra are limited to 600 nm.

Table 2. Stokes Shifts at 298 and 77 K^a

dye	$\lambda_{0-0}(\text{abs})/\lambda_{0-0}(\text{em})$	Stokes shift Δ (cm ⁻¹)		
		298 K	$\lambda_{0-0}(\text{abs})/\lambda_{0-0}(\text{em})$	77 K
[Fb]				
1	648/651	70 (F)	641/644	75 (F)
4	648/652	95 (F)	640/645	120 (F)
[Pdporph]				
2	554/601	140 (F)	554/601	140 (F)
	554/700	3760 (P)	554/685	3450 (P)
3	554/603	145 (F)	554/602	145 (F)
	554/701	3790 (P)	554/686	3340 (P)
5	554/602	145 (F)	554/603	145 (F)
	554/700	3765 (P)	554/686	3470 (P)

^aThe uncertainties on λ are ± 2 nm. F = fluorescence; P = phosphorescence.

fluorescence of a free base porphyrin (at 652 and 719 nm, plus a shoulder at ~ 780 nm). This assignment is supported by

Table 1. UV–vis Absorption Data in 2-MeTHF at 298 K.

dye	λ_{max} nm ($\epsilon, \times 10^3 \text{ M}^{-1} \cdot \text{cm}^{-1}$)				
	Soret band	Q bands			
[Fb]					
1	418 (414.4)	514 (18.6)	549 (9.3)	592 (5.3)	648 (4.2)
4	418 (318.4)	515 (18.6)	550 (9.9)	592 (5.5)	648 (4.4)
[Pdporph]					
2	416 (303.0)	523 (27.5)	554 (2.4)		
3	416 (249.2)	524 (26.4)	554 (2.5)		
5	416 (248.9)	523 (26.8)	554 (2.6)		

Table 3. Fluorescence Lifetimes, τ_F , in 2-MeTHF^a

dye	298 K			77 K		
	λ_{exc} (nm)	λ_F (nm)	τ_F (ns)	Φ_F (%)	λ_F (nm)	τ_{em} (ns)
[Fb]						
1	510	651 / 718	14.5 ± 0.2	12.0	644	10.8 ± 0.2
4	510	652 / 719	10.4 ± 0.2	4.4	645	9.5 ± 0.2
	λ_{exc} (nm)	λ_P (nm)	τ_P (μ s)	Φ_{em} (%) ^b	λ_P (nm)	τ_P (μ s)
[Pdporph]						
2	510	700 / 774	101.0 ± 1.5	6.9	685	1335 ± 20
3	510	701 / 773	28.5 ± 0.5	0.8	686	1350 ± 20
5	510	700 / 773	8.9 ± 0.5	0.2	686	1160 ± 20

^aThe fluorescence lifetimes, τ_F , for 2, 3, and 5 are < 150 ps (detection limit). ^bThe quantum yields include the sum of both the fluorescence and phosphorescence.

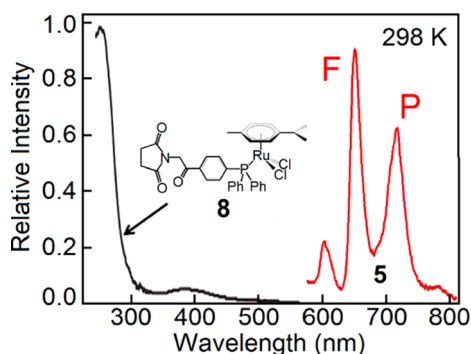


Figure 4. Comparison of the absorption spectrum of **8** (as potential acceptor) with the emission spectrum of **5** (as potential energy donor) in 2-MeTHF at 298 K in order to qualitatively demonstrate that the J-integral is nil.

the small Stoke shifts (Table 2, Δ ; difference between the 0–0 peaks measured in the absorption and emission spectra) here ranging from 70 to 120 cm^{-1} , and the common size for the fluorescence lifetime (τ_F) ordinarily ranging from 10 to 15 ns (Table 3).²⁰ Conversely, the [Pdporph]-containing species **2**, **3** and **5**, exhibit both a weak fluorescence (two bands in the 600–670 nm window) and a strong phosphorescence particularly pronounced at 77 K (two peaks in the 680–850 nm window), again based on the same metrics used for **1** and **4**.^{20,21} Indeed, the τ_F and Δ are, respectively, <150 ps (detection limit) and 145 cm^{-1} for the fluorescence and are in the μ s time scale and $\sim 3600 \pm 190 \text{ cm}^{-1}$ for the phosphorescence.

For the purpose of this work, the relative intensity is a key issue. The ligands exhibit reasonable emission quantum yields, Φ_F (12% for **1**) and Φ_P ($\sim 7\%$ for **2**). However, a decrease is noted in both Φ_F (from 12 to 4.4%; factor of ~ 2.7) and τ_F (from 14.5 to 10.4 ns; decrease of 28%) when a metal center, [M] (here [M] = [Ru(η^6 -p-cymene)Cl₂] = [Ru]) going from **1** to **4**. The decrease in τ_F is fully consistent with the loose bolt effect.²² As the mass of the side arm substituent increases, k_{ic} (nonradiative rate constant for internal conversion) also increase. Moreover, the presence of the [Ru] pendant group should promote the heavy atom effect, which in turn should increase k_{isc} (nonradiative rate constant for intersystem crossing).²² Notably, both effects impact on these photophysical parameters in the same direction. However, both τ_F and Φ_F should vary proportionally because $1/\tau_F = k_F + k_{ic} + k_{isc}$ and $1/\Phi_F = k_F/(k_F + k_{ic} + k_{isc})$, where k_F is the radiative rate constant for fluorescence (the photoreactions excluded from these expressions), but this is not the case. The decrease in Φ_F

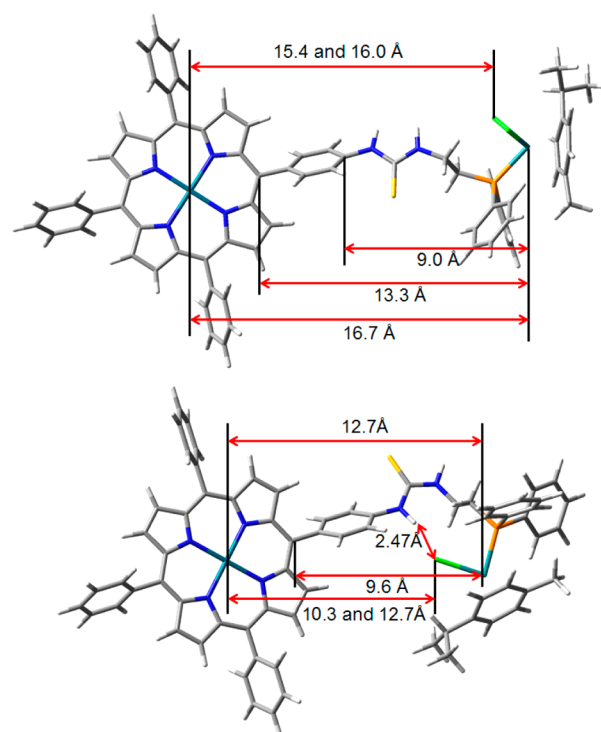


Figure 5. Computer modeling of complexes **3** and **5** (note that it also applies for **4**). Top: unfolded. Bottom: folded conformation due to the presence of an intramolecular H-bond). The dark turquoise, green, and light turquoise atoms are the palladium(II), chloride, and metal (Ru or Os), respectively.

by 2.7 fold going from **1** to **4** is rather curious, and one may conclude that there are some specific interactions occurring. These trends (i.e., first, decreases in the photophysical metrics when [M] is coordinated onto the ligand, and second, disproportion in the decreases of Φ_P and τ_P) are also noted for **3** ([M] = [Os(η^6 -p-cymene)Cl₂] = [Os]) and **5** ([M] = [Ru(η^6 -p-cymene)Cl₂] = [Ru]). The interpretation of the data is a little more complicated in the series **2** versus **3** versus **5**. Indeed, the heavy atom effect should be more pronounced for **3** ([Os]) than for **5** ([Ru]), and yet both τ_P and Φ_{em} are smaller for **5** than for **3**. To explain these observations, energy, atom, and electron transfers are now considered. For the S₁ and T₁ energy transfer processes (i.e., [Fb]* and [Pdporph]* → [Ru] and [Os]), the model complex **8** were investigated (Chart 2). Two mechanisms are possible: Förster (occurring via

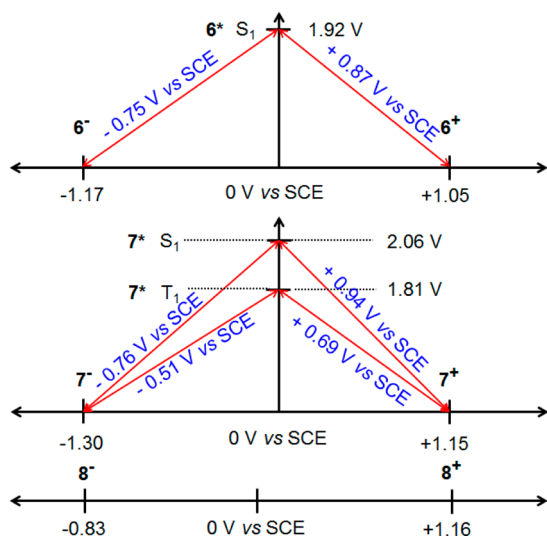


Figure 6. Modified Latimer diagram for a one-electron transfer for complexes 4 and 5 using the model species 6, 7, and 8. The excited state energies are those of the 0–0 peaks observed in the fluorescence and phosphorescence spectra of 4 and 5 at 77 K (where there is no or almost no contribution from hot bands rendering the evaluation of the pure electronic transition more accurate). The oxidation and reduction potentials are those from Table 4, and the approximated driving forces for a one-electron transfer are noted in blue.

Coulombic interactions)²³ and Dexter (occurring via double electron exchange).²⁴

The rate of the Förster energy transfer ($k_{\text{Förster}}$) can be described by eq 1 where $\Phi_{\text{F}}^{\circ}(\text{D})$ and $\tau_{\text{F}}^{\circ}(\text{D})$ are, respectively, the fluorescence quantum yield and lifetime of the donor in the absence of an acceptor, κ is an orientation factor associated with the relative alignment of the transition dipole moments of the donor and acceptor, r is the center-to-center donor–acceptor distance, n is the medium refractive index, $(\int F_{\text{D}}(\lambda)\epsilon_{\text{A}}(\lambda)\lambda^4 d\lambda) / (\int F_{\text{D}}(\lambda)d\lambda)$ (also called J -integral) is the normalized spectral overlap between the donor emission and the acceptor absorption (F_{D} = donor fluorescence intensity, ϵ_{A} = acceptor absorptivity, λ = wavelength), and N_{a} is Avogadro's number.

$$k_{\text{ET}} = \frac{\Phi_{\text{F}}^{\circ}(\text{D})\kappa^2 \left(\frac{9000(\ln 10)}{128\pi^5 n^4 N_{\text{a}}} \right) \int F_{\text{D}}(\lambda)\epsilon_{\text{A}}(\lambda)\lambda^4 d\lambda}{\tau_{\text{F}}^{\circ}(\text{D})r^2 \int F_{\text{D}}(\lambda)d\lambda} \quad (1)$$

The rate of a Dexter electron exchange (k_{Dexter}) is given by $k_{\text{ET}}(\text{Dexter}) = KJ \exp(-2r/L)$ where K is a pre-exponential factor that describes the degree of orbital interaction, L is the sum of the Van de Waals radii of the donor and acceptor, and J is the same spectral overlap between the donor emission and the acceptor absorption above.

As a typical example, the comparison of the absorption spectrum of the acceptor, here modeled by complex 8, with that of the fluorescence and phosphorescence of complex 5

(assuming that the [Pdporph] chromophore can act as an energy donor) shows a clear lack of spectral overlap (Figure 4). Because of the very strong spectral similarity of the other chromophores, the same conclusions apply, and the assumption that S_1 and T_1 energy transfer processes from [Fb]* and [Pdporph]* to [Ru] and [Os] are most unlikely.

For probing the possibility that an atom transfer occurs in the excited states of 3–5, computer modeling was performed. The weakest and unhindered bond in the [M] fragment is unquestionably the M–Cl one, and consequently one should investigate any short distance Cl...atom interactions since proximity is the key factor that would favor (or not) this excited state deactivation process. The lowest energy conformation is the completely unfolded geometry (Figure 5, top). Any Cl...atom separations with various atoms in the [Pdporph] chromophore (i.e., Pd, meso-C, and para-C of the phenyl group, for examples) will exceed the sum of their corresponding van der Waals radii (3.35 Å for Cl...C; 3.38 Å for Cl...Pd). In this conformation, atom transfer is simply impossible.

A second conformation with a local minimum was noticed during the computer modeling and exhibit a folded geometry driven by the presence of an intramolecular H-bond between the M–Cl unit and H–N group (the calculated Cl...H distance is ~ 2.47 Å; which is under the sum of the van der Waals radii, 2.95 Å, and under the sum of the covalent radii, 1.34 Å) (Figure 5, bottom). Despite this geometry, the Cl...atom separations between the Cl ligand and any key atom of the dye are still unreasonably too long for any transfer between the two units. Moreover, no photodegradation of the complexes was observed during prolonged exposure to light (in this work all analysis was performed at 510 nm). This means that, experimentally, the photoinduced atom transfer simply did not occur. However, the observation of a folded conformation with a local minimum brings interesting information about a slight shortening of the Pd...M distance when going from unfolded to folded geometry from 16.7 to 12.7 Å.

The last possible process to consider is the electron transfer. In order to address the situation, one must evaluate the driving force for both photoinduced oxidative and reductive electron transfer of the [Fb] and the [Pdporph] chromophores. Modified Latimer diagrams are constructed below after describing the electrochemistry of three model compounds 6–8.

Electrochemistry. The cyclic voltammogram of 6, 7, and 8 (model compounds) were studied in CH_2Cl_2 0.1 M TBAPF₆. This solvent has been chosen because it solubilizes the studied compounds and offers a wide potential window. The model compounds 6 and 7 were selected because they were readily available as they were used as chemical intermediates during the synthesis of the target complexes 3, 4, and 5. Although the remotely placed thiourea function from the central redox center (i.e., porphyrin ring) is not identical to the NO₂ group, both

Table 4. Potential Values of 6, 7, 8 and Ferrocene in CH_2Cl_2 0.1 M TBAPF₆ in V vs SCE

products	3rd reduction	2nd reduction	1st reduction	1st oxidation	2nd oxidation
6	−1.800 ^a	~ −1.275 ^a	−1.165 ^a	1.045 (90) ^b	1.360 (90) ^b
7		−1.300 ^a	−1.165 ^a	1.150 (85) ^b	1.565 (85) ^b
8	−1.780 ^a	~ −1.030 ^a	~ −0.825 ^a	1.160 (85) ^b	
ferrocene				0.440 (85) ^b	

^a E_{pc} irreversible system. ^b $E_{1/2}$, reversible system, ΔE_{p} values ($\Delta E_{\text{p}} = E_{\text{pa}} - E_{\text{pc}}$) are given in brackets (in mV).

exhibit electron-withdrawing properties thought to be the resonance structures of the thiourea ($\text{HN}-\text{C}=\text{S} \leftrightarrow \text{HN}^+=\text{C}-\text{S}^-$). It is reasonably assumed that the redox properties of the central porphyrin macrocycle would be relatively unaltered by this difference.

In the positive potential range, **6** and **7** exhibit two mono-electronic reversible oxidations leading, respectively, to the cation radical and the dication (the cyclic voltammograms are placed in the SI).²⁵ As expected, the palladium complex **7** is harder to oxidize than the free base **6** due to its electron-withdrawing effect on the porphyrin macrocycle. The ruthenium complex **8** exhibits only one reversible mono-electronic oxidation at 1.16 V versus SCE, which corresponds to the Ru(II) \rightarrow Ru(III) electron transfer. A similar oxidation potential (1.14 V vs. SCE) was previously reported for the very similar $[\text{Ru}(\eta^6\text{-}p\text{-cymene})\text{Cl}_2(\text{PPh}_3)]$ complex.²⁶

In the negative potential range, the free base porphyrin **6** is irreversibly reduced in three steps. The first one likely corresponds to the first porphyrin reduction because the gap between its first oxidation and reduction, $\Delta E(\text{ox1} - \text{red1}) = 2.21$ V, matches well with those found for common porphyrins (2.15 ± 0.15 V).²⁵ The second reduction might correspond to the reduction of the nitro group,²⁷ although it is difficult to assign precisely the third reduction. The redox behavior of the palladium complex **7** is simpler with a first reversible mono-electronic reduction of the porphyrin core occurring at -1.165 V. The second reversible redox system is observed at -1.30 V, a potential similar to the one observed for the second reduction of the free base **6** (-1.275 V) and corresponds thus probably to the reduction of the nitro group. The cyclic voltammogram of the ruthenium complex **8** exhibits very broad and ill-defined reduction peaks. Nonetheless, modified Latimer diagrams are constructed, and the driving forces for a reductive or oxidative one-electron process are indicated in blue (Figure 6).

The four probed possible processes from these diagrams are the following:



and



The oxidation of Ru(II) into Ru(III) occurs at $+1.16$ V vs SCE. The driving forces for the photoinduced reduction of $[\text{Fb}]^*(\text{S}_1) + 1\text{-e}^-$ into $[\text{Fb}]^-$, $[\text{Pdporph}]^*(\text{S}_1) + 1\text{-e}^-$ into $[\text{Pdporph}]^-$, and $[\text{Pdporph}]^*(\text{T}_1) + 1\text{-e}^-$ into $[\text{Pdporph}]^-$ are simply not large enough to render these processes thermodynamically favorable. Similarly, model complex **8** can be reduced to **8⁻** at -0.83 V vs SCE. The modified Latimer diagrams indicate that only the photoinduced oxidation of $[\text{Fb}]^*(\text{S}_1)$ into $[\text{Fb}]^+ + 1\text{-e}^-$, $[\text{Pdporph}]^*(\text{S}_1)$ into $[\text{Pdporph}]^+ + 1\text{-e}^-$ can be favorable with a very low energy release of ~ 0.04 (~ 3.9) and ~ 0.11 V (i.e., ~ 11 kJ/mol). By neglecting the reorganization energy for the transition from a neutral species to a zwitterionic charge separated state, and considering the long separation between the two units (dye and $[\text{M}]$) based on

computer modeling, at first glance, the quenching from a photoinduced electron transfer, if any, appears to be bound to be slow or very slow. This conclusion is supported by the absence of a strong quenching of the dye fluorescence. Indeed, by estimating its rate, k_{et} , using $k_{\text{et}} = (1/\tau_{\text{F}}) - (1/\tau_{\text{F}}^{\circ})$ where τ_{F} and τ_{F}° are the fluorescence lifetimes of the donor (here $[\text{Fb}]$) in the presence (**4**) and absence (**1**) of an electron acceptor, one finds $k_{\text{et}} \sim 2.7 \times 10^7$ at 298 and $\sim 1.3 \times 10^7$ s⁻¹ at 77 K (data from Table 3). Although the decrease in k_{et} upon cooling (i.e., rendering the medium more rigid) is consistent with the expected increase in reorganization energy, the size of these presumed k_{et} 's is the same as what we find for k_{ic} .²² Consequently all of the arguments above, specifically neglecting the reorganization energy, long separation between the dye and $[\text{M}]$, and very small estimated k_{et} 's, indicate that this process can certainly be neglected. Because of the very short τ_{F} values for $[\text{Pdporph}]$ (< 150 ps), it is not possible to address this issue for this specific chromophore.

More importantly, because these modified Latimer diagrams unambiguously indicate that the photoinduced electron transfer is not thermodynamically favorable in the triplet state, the question is what then quenches the phosphorescence of the $[\text{Pdporph}]$ unit when $[\text{Ru}]$ and $[\text{Os}]$ are coordinated onto ligand **2**. Moreover, although a decrease in τ_{p} is noted at 298 K going from ligand **2** to the complexes **3** and **5**, why is this decrease not observed at 77 K? At this point, only circumstantial evidence can be provided.

Computer modeling permitted to detect the presence of a folded conformation at higher energy (*vide infra*). This means upon Brownian motions both geometries are accessible, and consequently, the photophysical parameters represent a weighted mixture associated with each conformation. Upon cooling the solution by pouring N₂(l) inside the Dewar, the sample experiences a decrease in the available thermal energy (kT; from 2.48 down to 0.64 kJ/mol), and so, only the unfolded geometry is favored in all cases and are frozen in the glassy matrix. The quasi-identical τ_{p} data for ligand **2** and complex **5** (Table 3) confirms this hypothesis (i.e., the metal atom is far away from the $[\text{Pdporph}]$ chromophore). Upon warming the solution back to 298 K, the τ_{p} data return to their initial state, so the process is reversible. More importantly, no quenching of the emission spectra are noted when $[\text{M}] = \text{AuCl}$,²⁰ meaning absence of the heavy atom effect. The presence of an H-bond driven folding is easily demonstrated by the absence of intramolecular H-bond with the thiourea center in the corresponding gold(I) complex presented in Chart 3 (as the P–Au–Cl angle is $\sim 180^\circ$ with no possibility of N–H \cdots Cl interactions).

CONCLUSION

Although ligands **1** and **2** exhibit reasonable emission intensity for imaging purposes, the anchoring of $[\text{M}]$ reduces the emission intensity and lifetimes, especially for **3** and **5**. Although it was clearly established that the dye– $[\text{M}]$ interactions do not involve any of the three classic quenching processes (energy, atom, or electron transfer), it became evident that the presence of a heavy atom near the chromophore can actually induce this effect. The proximity of the two fragments is achieved by the folding of the flexible chain, toward an uphill energy conformations stabilized by an H-bond (N–H \cdots Cl–M). This work permitted the discovery of a new feature to consider when designing bimetallic

theranostics. It may be preferable to use rigid spacers separating the dye from the metallic center.

■ ASSOCIATED CONTENT

■ Supporting Information

HRMS (MALDI/TOF) mass spectra of compound 1–5 (Figures S1–S9), ^1H , ^{31}P , and ^{13}C NMR spectra of compounds (Figures S10–S21), cyclic voltammograms of compounds 6–8 (Figures S22–S24), synthesis of porphyrin 1, 2, 6, and 7 and compound 8 (S25), UV–visible stability study of 3 and 5 (Figures S26–S27), crystal data and structure refinement for 8 (Table S28). This material is available free of charge via the Internet at <http://pubs.acs.org>.

■ AUTHOR INFORMATION

Corresponding Authors

*E-mail: pierre.harvey@USherbrooke.ca. Tel.: 819-821-7092. Fax: 819-821-8017.

*E-mail: claud.gros@u-bourgogne.fr. Tel.: 33 (0)3 80 39 61 12.

*E-mail: ewen.bodio@u-bourgogne.fr. Tel.: 33 (0)3 80 39 60 76.

Notes

The authors declare no competing financial interest.

■ ACKNOWLEDGMENTS

The *Centre National de la Recherche Scientifique* (ICMUB, UMR CNRS 6302) is gratefully thanked for financial support. Support was provided by the CNRS, the *Université de Bourgogne* and the *Conseil Régional de Bourgogne* through the 3MIM integrated project (*Marquage de Molécules par les Métaux pour l'Imagerie Médicale*). S.T. thanks the French Ministry of Research for PhD scholarship. P.D.H. thanks the *Agence Nationale de la Recherche (ANR)* and the Sciences and Engineering Research Council of Canada (NSERC) for financial support. Fanny Picquet and Marie José Penouilh are warmly acknowledged for technical support. We are thankful to Dr. Margot Wenzel for the X-ray structure of compound 8.

■ REFERENCES

- (1) (a) Bardhan, R.; Lal, S.; Joshi, A.; Halas, N. J. *Acc. Chem. Res.* **2011**, *44*, 936–946. (b) Kelkar, S. S.; Reineke, T. M. *Bioconjugate Chem.* **2011**, *22*, 1879–1903.
- (2) Arrowsmith, R. L.; Pascu, S. I.; Smugowski, H. *Organomet. Chem.* **2012**, *38*, 1–35.
- (3) (a) Nazarov, A.; Hartinger, C. G.; Dyson, P. J. *J. Organomet. Chem.* **2014**, *751*, 251–260. (b) Clavel, C. M.; Paunescu, E.; Nowak-Sliwiska, P.; Griffioen, A. W.; Scopelliti, R.; Dyson, P. J. *J. Med. Chem.* **2014**, *57*, 3546–3558. (c) Allardyce, C. S.; Dyson, P. J.; Ellis, D. J.; Heath, S. L. *Chem. Commun.* **2001**, 1396–1397. (d) Ang, W. H.; Daldini, E.; Juillerat-Jeanneret, L.; Dyson, P. J. *Inorg. Chem.* **2007**, *46*, 9048–9050. (e) Casini, A.; Edafe, F.; Erlandsson, M.; Gonsalvi, L.; Ciancetta, A.; Re, N.; Ienco, A.; Messori, L.; Peruzzini, M.; Dyson, P. J. *Dalton Trans.* **2010**, 39, 5556–5563. (f) Casini, A.; Gabbiani, C.; Sorrentino, F.; Rigobello, M. P.; Bindoli, A.; Geldbach, T. J.; Marrone, A.; Re, N.; Hartinger, C. G.; Dyson, P. J.; Messori, L. *J. Med. Chem.* **2008**, *51*, 6773–6781. (g) Castonguay, A.; Doucet, C.; Juhas, M.; Maysinger, D. *J. Med. Chem.* **2012**, *55*, 8799–8806. (h) Dorcier, A.; Ang, W. H.; Bolaño, S.; Gonsalvi, L.; Juillerat-Jeanneret, L.; Laurenczy, G.; Peruzzini, M.; Phillips, A. D.; Zanobini, F.; Dyson, P. J. *Organometallics* **2006**, *25*, 4090–4096. (i) Dorcier, A.; Dyson, P. J.; Gossens, C.; Rothlisberger, U.; Scopelliti, R.; Tavernelli, I. *Organometallics* **2005**, *24*, 2114–2123. (j) Dutta, B.; Scolaro, C.; Scopelliti, R.; Dyson, P. J.; Severin, K. *Organometallics* **2008**, *27*, 1355–1357.

- (k) Govender, P.; Edafe, F.; Makhubela, B. C. E.; Dyson, P. J.; Therrien, B.; Smith, G. S. *Inorg. Chim. Acta* **2014**, *409*, 112–120.
- (l) Komeda, S.; Casini, A. *Curr. Top. Med. Chem.* **2012**, *12*, 219–235.
- (m) Renfrew, A. *Chimia* **2009**, *63*, 217–219. (n) Renfrew, A. K.; Phillips, A. D.; Egger, A. E.; Hartinger, C. G.; Bosquain, S. S.; Nazarov, A. A.; Keppler, B. K.; Gonsalvi, L.; Peruzzini, M.; Dyson, P. J. *Organometallics* **2009**, *28*, 1165–1172. (o) Scolaro, C.; Bergamo, A.; Brescacin, L.; Delfino, R.; Cocchietto, M.; Laurenczy, G.; Geldbach, T. J.; Sava, G.; Dyson, P. J. *J. Med. Chem.* **2005**, *48*, 4161–4171. (p) Scolaro, C.; Geldbach, T. J.; Rochat, S.; Dorcier, A.; Gossens, C.; Bergamo, A.; Cocchietto, M.; Tavernelli, I.; Sava, G.; Rothlisberger, U.; Dyson, P. *Organometallics* **2006**, *25*, 756–765. (q) Vock, C. A.; Ang, W. H.; Scolaro, C.; Phillips, A. D.; Lagopoulos, L.; Juillerat-Jeanneret, L.; Sava, G.; Scopelliti, R.; Dyson, P. J. *J. Med. Chem.* **2007**, *50*, 2166–2175.
- (4) (a) Dyson, P. J.; Sava, G. *Dalton Trans.* **2006**, 1929–1933. (b) Groessl, M.; Reisner, E.; Hartinger, C. G.; Eichinger, R.; Semenova, O.; Timerbaev, A. R.; Jakupec, M. A.; Arion, V. B.; Keppler, B. K. *J. Med. Chem.* **2007**, *50*, 2185–2193.
- (5) (a) Hartinger, C. G.; Hann, S.; Koellensperger, G.; Sulyok, M.; Groessl, M.; Timerbaev, A. R.; Rudnev, A. V.; Stingeder, G.; Keppler, B. K. *Int. J. Clin. Pharmacol. Ther.* **2005**, *43*, 583–585. (b) Timerbaev, A. R.; Hartinger, C. G.; Aleksenko, S. S.; Keppler, B. K. *Chem. Rev.* **2006**, *106*, 2224–2248. (c) Schluga, P.; Hartinger, C. G.; Egger, A.; Reisner, E.; Galanski, M.; Jakupec, M. A.; Keppler, B. K. *Dalton Trans.* **2006**, 1796–1802. (d) Casini, A.; Mastrobuoni, G.; Terenghi, M.; Gabbiani, C.; Monzani, E.; Moneti, G.; Casella, L.; Messori, L. *J. Biol. Inorg. Chem.* **2007**, *12*, 1107–1117. (e) Scolaro, C.; Chaplin, A. B.; Hartinger, C. G.; Bergamo, A.; Cocchietto, M.; Keppler, B. K.; Sava, G.; Dyson, P. J. *Dalton Trans.* **2007**, 5065–5072.
- (6) (a) Adhikreksan, Z.; Davey, G. E.; Campomanes, P.; Groessl, M.; Clavel, C. M.; Yu, H.; Nazarov, A. A.; Yeo, C. H. F.; Ang, W. H.; Drøge, P.; Rothlisberger, U.; Dyson, P. J.; Davey, C. A. *Nat. Commun.* **2014**, *5*, 3462. (b) Pelletier, F.; Comte, V.; Massard, A.; Wenzel, M.; Toulot, S.; Richard, P.; Picquet, M.; Le, G. P.; Zava, O.; Edafe, F.; Casini, A.; Dyson, P. J. *J. Med. Chem.* **2010**, *53*, 6923–6933. (c) Hartinger, C. G.; Casini, A.; Duhot, C.; Tsybin, Y. O.; Messori, L.; Dyson, P. J. *J. Inorg. Biochem.* **2008**, *102*, 2136–2141.
- (7) (a) Ishikawa, T.; Ali-Osman, F. *J. Biol. Chem.* **1993**, *268*, 20116–20125. (b) Sava, G.; Bergamo, A.; Zorzet, S.; Gava, B.; Casarsa, C.; Cocchietto, M.; Furlani, A.; Scarcia, V.; Serli, B.; Iengo, E.; Alessio, E.; Mestroni, G. *Eur. J. Cancer* **2002**, *38*, 427–435. (c) Fokkema, E.; Groen, H. J. M.; Helder, M. N.; de Vries, E. G. E.; Meijer, C. *Biochem. Pharmacol.* **2002**, *63*, 1989–1996. (d) Jansen, B. A. J.; Brouwer, J.; Reedijk, J. J. *Inorg. Biochem.* **2002**, *89*, 197–202. (e) Wang, F.; Xu, J.; Habtemariam, A.; Bella, J.; Sadler, P. J. *J. Am. Chem. Soc.* **2005**, *127*, 17734–17743. (f) Papadia, P.; Margiotta, N.; Bergamo, A.; Sava, G.; Natile, G. *J. Med. Chem.* **2005**, *48*, 3364–3371. (g) Bali, M. S.; Buck, D. P.; Coe, A. J.; Day, A. L.; Collins, J. G. *Dalton Trans.* **2006**, 5337–5344. (h) Yangyuoru, P. M.; Webb, J. W.; Shaw, C. F., III. *J. Inorg. Biochem.* **2008**, *102*, 584–593. (i) Heffeter, P.; Jungwirth, U.; Jakupec, M.; Hartinger, C.; Galanski, M.; Elbling, L.; Micksche, M.; Keppler, B.; Berger, W. *Drug Res. Upd.* **2008**, *11*, 1–16.
- (8) (a) Nyman, E. S.; Hynninen, P. H. *J. Photochem. Photobiol., B* **2004**, *73*, 1–28. (b) O'Connor, A. E.; Gallagher, W. M.; Byrne, A. T. *Photochem. Photobiol.* **2009**, *85*, 1053–1074. (c) Vicente, M. G. H. *Curr. Med. Chem.: Anti-Cancer Agents* **2001**, *1*, 175–194.
- (9) (a) Ethirajan, M.; Chen, Y.; Joshi, P.; Pandey, R. K. *Chem. Soc. Rev.* **2011**, *40*, 340–362. (b) Josefsen, L. B.; Boyle, R. W. *Theranostics* **2012**, *2*, 916–966. (c) Zhang, Y.; Lovell, J. F. *Theranostics* **2012**, *2*, 905–915.
- (10) Sun, R. W.-Y.; Che, C.-M. *Coord. Chem. Rev.* **2009**, *253*, 1682–1691.
- (11) (a) Hirohara, S.; Kawasaki, Y.; Funasako, R.; Yasui, N.; Totani, M.; Alitomo, H.; Yuasa, J.; Kawai, T.; Oka, C.; Kawaichi, M.; Obata, M.; Tanihara, M. *Bioconjugate Chem.* **2012**, *23*, 1881–1890. (b) Rubio, N.; Prat, F.; Bou, N.; Borrell, J. I.; Teixido, J.; Villanueva, A.; Juarranz, A.; Canete, M.; Stockert, J. C.; Nonell, S. *New J. Chem.* **2005**, *29*, 378–384.

(12) Tsekova, D.; Gorolomova, P.; Gochev, G.; Skumryev, V.; Momekov, G.; Momekova, D.; Gencheva, G. *J. Inorg. Biochem.* **2013**, *124*, 54–62.

(13) (a) Tasan, S.; Licon, C.; Michelin, C.; Doulain, P.-E.; Gros, C. P.; Picquet, M.; Le Gendre, P.; Harvey, P. D.; Paul, C.; Gaiddon, C.; Bodio, E. *Dalton Trans.* **2015**, *20*, 143–154. (b) see SI of the following article: Tasan, S.; Zava, O.; Bertrand, B.; Bernhard, C.; Goze, C.; Picquet, M.; Le Gendre, P.; Harvey, P.; Denat, F.; Casini, A.; Bodio, E. *Dalton Trans.* **2013**, *42*, 6102–6109.

(14) Nifiatis, F.; Athas, J. C.; Gunaratne, K. D. D.; Gurung, Y.; Monette, K. M.; Shivokevich, P. J. *Open Spectrosc. J.* **2011**, *5*, 1–12.

(15) Frisch, M. J.; Trucks, G. W.; Schlegel, H. B.; Scuseria, G. E.; Robb, M. A.; Cheeseman, J. R.; Montgomery, Jr., J. A.; Vreven, T.; Kudin, K. N.; Burant, J. C.; Millam, J. M.; Iyengar, S. S.; Tomasi, J.; Barone, V.; Mennucci, B.; Cossi, M.; Scalmani, G.; Rega, N.; Petersson, G. A.; Nakatsuji, H.; Hada, M.; Ehara, M.; Toyota, K.; Fukuda, R.; Hasegawa, J.; Ishida, M.; Nakajima, T.; Honda, Y.; Kitao, O.; Nakai, H.; Klene, M.; Li, X.; Knox, J. E.; Hratchian, H. P.; Cross, J. B.; Bakken, V.; Adamo, C.; Jaramillo, J.; Gomperts, R.; Stratmann, R. E.; Yazyev, O.; Austin, A. J.; Cammi, R.; Pomelli, C.; Ochterski, J. W.; Ayala, P. Y.; Morokuma, K.; Voth, G. A.; Salvador, P.; Dannenberg, J. J.; Zakrzewski, V. G.; Dapprich, S.; Daniels, A. D.; Strain, M. C.; Farkas, O.; Malick, D. K.; Rabuck, A. D.; Raghavachari, K.; Foresman, J. B.; Ortiz, J. V.; Cui, Q.; Baboul, A. G.; Clifford, S.; Cioslowski, J.; Stefanov, B. B.; Liu, G.; Liashenko, A.; Piskorz, P.; Komaromi, I.; Martin, R. L.; Fox, D. J.; Keith, T.; Al-Laham, M. A.; Peng, C. Y.; Nanayakkara, A.; Challacombe, M.; Gill, P. M. W.; Johnson, B.; Chen, W.; Wong, M. W.; Gonzalez, C.; Pople, J. A. *Gaussian 09*; Gaussian, Inc.: Wallingford, CT, 2009.

(16) (a) Bauernschmitt, R.; Ahlrichs, R. *Chem. Phys. Lett.* **1996**, *256*, 454–464. (b) Becke, A. D. *J. Chem. Phys.* **1993**, *98*, 5648–5652. (c) Casida, M. E.; Jamorski, C.; Casida, K. C.; Salahub, D. R. *J. Chem. Phys.* **1998**, *108*, 4439–4449. (d) Hohenberg, P.; Kohn, W. *Phys. Rev.* **1964**, *136*, B864–871. (e) Hohenberg, P.; Kohn, W. *J. Phys. Rev.* **1965**, *140*, A1133–1138. (f) Lee, C.; Yang, W.; Parr, R. G. *Phys. Rev. B* **1988**, *37*, 785–789. (g) Miehlich, B.; Savin, A.; Stoll, H.; Preuss, H. *Chem. Phys. Lett.* **1989**, *157*, 200–206. (h) Parr, R. G.; Yang, W. *Density-functional theory of atoms and molecules*; Oxford University Press: Oxford, 1989. (i) *The Challenge of d and f Electrons: Theory and Computation*; Salahub, D. R., Zerner, M. C., Eds.; ACS Symposium Series; American Chemical Society: Washington, DC, **1989**; Chapter 21 (j) Stratmann, R. E.; Scuseria, G. E.; Frisch, M. J. *J. Chem. Phys.* **1998**, *109*, 8218–8224.

(17) (a) Binkley, J. S.; Pople, J. A.; Hehre, W. J. *J. Am. Chem. Soc.* **1980**, *102*, 939–947. (b) Dobbs, K. D.; Hehre, W. J. *J. Comput. Chem.* **1986**, *7*, 359–378. (c) Dobbs, K. D.; Hehre, W. J. *J. Comput. Chem.* **1987**, *8*, 861–879. (d) Dobbs, K. D.; Hehre, W. J. *J. Comput. Chem.* **1987**, *8*, 880–893. (e) Gordon, M. S.; Binkley, J. S.; Pople, J. A.; Pietro, W. J.; Hehre, W. J. *J. Am. Chem. Soc.* **1982**, *104*, 2797–2803. (f) Pietro, W. J.; Francl, M. M.; Hehre, W. J.; Defrees, D. J.; Pople, J. A.; Binkley, J. S. *J. Am. Chem. Soc.* **1982**, *104*, 5039–5048.

(18) Dolomanov, O. V.; Bourhis, L. J.; Gildea, R. J.; Howard, J. A. K.; Puschmann, H. *J. Appl. Crystallogr.* **2009**, *42*, 339–341.

(19) Sheldrick, G. M. *Acta Cryst. A* **2008**, *64*, 112–122.

(20) Harvey, P. D. In *Handbook on Porphyrins and Phthalocyanines*; Kadish, K. M., Guillard, R., Smith, K. M., Eds.; Elsevier Science: Amsterdam, 2003; Vol. 113, pp 63–249.

(21) Bolze, F.; Gros, C. P.; Harvey, P. D.; Guillard, R. *J. Porphyrins Phthalocyanines* **2001**, *5*, 569–574.

(22) (a) Turro, N. J. *Modern Molecular Photochemistry*; Benjamin/Cummings: Menlo Park, CA, 1978. (b) Turro, N. J.; Kochevar, I. F.; Nogguchi, Y.; Chow, M. F. *J. Am. Chem. Soc.* **1978**, *100*, 3170.

(23) (a) Forster, T. *Discuss. Faraday Soc.* **1959**, *27*, 7–17. (b) Förster, T. *Ann. Phys.* **1948**, *2*, 55–75.

(24) (a) Dexter, D. L. *J. Chem. Phys.* **1953**, *21*, 836–850. (b) Dexter, D. L. *J. Chem. Phys.* **1953**, *21*, 836–850.

(25) Kadish, K. M.; Van Caemelbecke, E.; Royal, G. In *The Porphyrin Handbook*; Kadish, K. M., Smith, K. M., Guillard, R., Eds.; Academic Press: San Diego, 2000; Vol. 8, pp 1–114.

(26) Marchetti, F.; Pettinari, C.; Cerquetella, A.; Cingolani, A.; Pettinari, R.; Monari, M.; Wanke, R.; Kuznetsov, M. L.; Pombeiro, A. J. L. *Inorg. Chem.* **2009**, *48*, 6096–6108.

(27) Devillers, C. H.; Hebié, S.; Lucas, D.; Cattey, H.; Clément, S.; Richeter, S. *J. Org. Chem.* **2014**, *79*, 6424–6434.